# EOSTAR: an electro-optical sensor performance model for predicting atmospheric refraction, turbulence, and transmission in the marine surface layer

Gerard J. Kunz*[a], Marcel M. Moerman[a], Alexander M.J. van Eijk[a],
Stephen M. Doss-Hammel[b] and Dimitri Tsintikidis[b],
[a]TNO Physics and Electronics Laboratory, Dept. of Electro-Optical Propagation and Signature Management, The Hague, The Netherlands,
[b]Atmospheric Propagation Branch, Code 2858,
SPAWAR Systems Center, San Diego, CA 92152, USA

## ABSTRACT

A first version of the integrated model EOSTAR (**E**lectro-**O**ptical **S**ignal **T**ransmission and **R**anging) to predict the performance of electro-optical (EO) sensor systems in the marine atmospheric surface layer has been developed. The model allows the user to define camera systems, atmospheric conditions and target characteristics, and it uses standard (shipboard) meteorological data to calculate atmospheric effects such as refraction, turbulence, spectrally resolved transmission, path- and background radiation. Alternatively, the user may specify vertical profiles of meteorological parameters and/or profiles of atmospheric refraction, either interactively or in data files with a flexible format. Atmospheric effects can be presented both numerically and graphically as distorted images of synthetically generated targets with spatially distributed emission properties. EOSTAR is a completely mouse-driven PC Windows program with a user-friendly interface and extended help files. Most calculations are performed in real-time, although spectral transmission and background radiation calculations take up to a few seconds for each new meteorological condition. The program can be used in a wide range of applications, e.g., for operational planning and instruction.

**Keywords**: electro-optical propagation, infrared, atmospheric refraction, turbulence, marine surface layer

## 1. INTRODUCTION

With the increasing use of long-range electro-optical (EO) sensors, especially in naval applications, there is a growing need to predict the performance of these sensors under different meteorological conditions. Currently, few if any models are available that provide all elements of the required information-chain. Thus there are models to predict turbulence in the marine surface layer[1,2,3,4], and there are models to predict the transmission and background radiation[5], both on the basis of standard (shipboard) meteorological data, but there is no software that couples these programs and presents the results in a convenient format.

Recognizing this problem, the TNO Physics and Electronics Laboratory, The Hague, The Netherlands and SPAWAR Systems Center San Diego, USA, started in 2001 the EOSTAR (Electro-Optical Signal Transmission and Ranging) project to calculate atmospheric effects on infrared (IR) imaging. The aim of the project is to develop a stand-alone PC-based computer code with a user-friendly interface, and fully user-definable input parameters. The initial design requirement was to drive the program from simple input parameters: standard meteorological data, available aboard a ship, and the necessary properties of the applied camera system. The first stage of the simulation is the solution of a number of micrometeorological models for the evaluation of the vertical profiles of temperature, humidity, and air

* Contact information: kunz@fel.tno.nl, phone: +31 70 374 0460, TNO Physics and Electronics Laboratory, P.O.Box 96864, 2509 JG The Hague, The Netherlands; http://www.tno.nl/instit/fel.

pressure in the marine surface layer, as well as, refraction and turbulence parameters. Subsequently, these data are used to calculate ray trajectories that simulate the instantaneous field-of-view of the individual camera pixels and which allow assessing atmospheric distortion, spectrally resolved path-integrated transmission, path and background radiance and optical turbulence.

In the second phase of the project, a module was added allowing the user to define targets in the scene. The user may control the geometry and radiative properties of the target in order to simulate realistic targets. Using the above information, it is now possible to simulate images as seen by the sensor with and without taking into account atmospheric effects.

The initial developments in the project have been reported previously[6]. Presently, two user-interfaces are being developed for the EOSTAR code. The first one focuses on the operational planning aspects, such as the assessment of the maximum detection range of a given target by a given sensor. This feature of EOSTAR will be discussed elsewhere. In this contribution, emphasis is placed on the second user-interface that aims to provide an understanding of the phenomena that cause image distortion and reduced sensor system performance. An overview is presented of the various modules in the code, and the current status of the project is described.

## 2. FRONT END

The objective of EOSTAR is to model the performance of EO sensor systems in the marine atmospheric surface layer, especially in the IR part of the electromagnetic spectrum. The input should be simple and limited to 1) properties of the selected camera, 2) current meteorological conditions such as wind speed, air and surface temperature, air pressure and humidity, and 3) a distant target. In addition, the program should run under Windows on standard PC's with an easily accessible user interface and sufficient help files (on-line access, demo-tours, etc).

To meet the first requirement, an input module was developed in which users can define their own camera specifications such as the spectral band, number and size of the pixels, noise performance and optical parameters. Secondary parameters, such as the field-of-view (FOV), the instantaneous-field-of-view (IFOV), theoretical point spread function and alternative parameters to express noise are calculated and presented instantaneously. Options are provided to store and retrieve the camera properties allowing to quickly change between different camera systems in a scene.

A second module was developed that handles the meteorological data and calculates the vertical profiles of wind speed, air temperature, humidity and pressure using micrometeorological bulk models. These models are based on the Monin-Obukhov similarity theory and are widespread[2,3,4,7,8,9]. In turn, this module calculates the vertical profiles of the atmospheric refractive index and the refractive index structure parameter, which are used to calculate the path integrated transmission losses and turbulence properties. The reliability of the program can be increased if additional information is provided such as the time of the day, geographical location, observation direction with respect to the sun, and cloud cover. At present, the module that handles the additional environmental information is partly integrated with the EOSTAR code and will be fully integrated in the near future.

To visualize atmospheric distortion effects in IR imagery, EOSTAR is equipped with a third module to simulate a number of (simple) targets, each constructed from sets of triangles. The triangles are associated with a number of properties such as geometry, temperature and spectral emission. Other properties can simply be added later on. The target module is being integrated with a signature calculation to evaluate the radiative properties of the target structural elements under specific atmospheric conditions. In the future, a tool will be added that handles user-defined targets from external data files.

## 3. INTERNAL PROCESSES

The EOSTAR program has a number of internal processes, which are sequentially activated each time one of the control parameters is changed. Thus when one of the meteorological or micrometeorological parameters is changed, all available bulk models are solved instantaneously and a new set of ray trajectories is calculated to define the viewing paths of the

various camera pixels. The latter calculation is also activated if one of the camera properties is changed. Subsequently, the program updates the atmospheric transfer functions, the scintillation and blur along the paths between the camera and the position of a user-selectable point source, and presents the updated distorted image of a selected distant target. The updated information is presented promptly without any noticeable delay. Spectrally resolved atmospheric transmission losses due to both molecules and aerosols are calculated using two separate programs (MODTRAN and ANAM, to be described later in the manuscript). However, these processes are relatively time-consuming. Therefore, several small internal look-up tables are prepared for the current meteorological condition, which are subsequently interpolated for further processing. With this approach, the time required to calculate the path-integrated transmission becomes comparable with the other processes in EOSTAR. The following sections provide some details of the internal processes within EOSTAR.

### 3.1 Meteorological input

As mentioned above, EOSTAR utilizes bulk models to calculate vertical meteorological profiles on the basis of simple standard observations. EOSTAR is provided with three different micrometeorological models[2,3,4] and with two different sets of stability functions[10,11]. In addition, users can define their own exchange coefficients to meet their specific requirements. This particular set-up comprises the **T**urbulence **A**nd **R**efraction **M**odeling **O**ver the **S**ea (TARMOS) model[12] used previously[6], but extends the options and offers more flexibility. Each of the six models is solved instantaneously using the given input parameters. The bulk module calculates and presents a large number of results such as the wind speed, temperature and humidity at the standard height of 10 m, the scaling parameters and roughness lengths for wind speed, temperature and humidity, and Monin-Obukhov length. Results are simultaneously available for all six models and a comparison of individual results can be helpful for detailed studies. The performance of the various bulk models in the module has been verified[12] with data available from literature, in particular Smith's model[2].

The user must select one particular model and only the data from that model are used for further calculations. The calculated profiles of the meteorological parameters are displayed graphically together with the selected input parameters. An example of (part of) the output of the bulk module is presented in the upper left panel of Figure 1. Atmospheric structure function parameters ($C_T^2$, $C_{Tq}$, $C_q^2$ and $C_n^2$) are calculated using the scaling parameters $u_*$, $T_*$ and $q_*$, also provided by the micrometeorological model[13] and the dependence of the refractive index on temperature and humidity ($dn/dT$ and $dn/dq$). Functions describing the height dependence can be found in the literature[14,15].

Although bulk models are commonly accepted and very useful, the atmospheric conditions in the surface layer cannot always be perfectly described by these models. There are situations that users prefer to work with measured or synthetic meteorological profiles to study more complex situations. For this purpose, EOSTAR is provided with a special module, which allows users to construct or read their own vertical profiles of temperature, humidity, wind speed, and refractive index (see the upper panel of Figure 2 for an example). However, at this time no information on turbulence parameters can be calculated when this mode is used.

The meteorological input module has provisions to store and read user-defined data for individual calculations, as well as to read and process large data files for multiple (sequential) calculations (e.g., to process trial information). The data format of these files is very flexible.

### 3.2 Ray trajectories

EOSTAR uses the meteorological data and Edléns model[16,17] for the refractive index of air to calculate the vertical profile of the atmospheric refractive index. A ray tracer is then used to infer the view or 'ray trajectories' of individual camera pixels. Two different approaches can be used: 1) Snell's law for spherically layered structures[18,19,20] and 2) the parabolic ray approach[21,22]. The two approaches yield nearly similar results, but the parabolic approach requires somewhat less computational time. Updating of the ray trajectories requires very limited computer time and is therefore done automatically after changing one of the meteorological or camera properties. The ray trajectories are presented in a 'height above the surface' versus range chart (see the upper right panel of Figure 1).

The ray trajectory calculation permits assessment of image distortion due to atmospheric refraction. Atmospheric refraction becomes important for long range observations and/or under special conditions. Well-known are the mirage effects over roads and Fata Morgana's in desert environments[21,23,24,25]. Similar effects occur over the ocean, hampering identification and affecting the maximum visibility ranges of objects. Examples of synthesized images in a non-refracting and in a refracting atmosphere are presented in the lower panels of Figure 1 respectively. Contour lines around the elementary triangles are shown to emphasize the individual elements of the target.

Ray trajectories are cut off when they reach the height of the wave crests. To this end, the wave field is represented as a 8th order fully developed Stokes wave with amplitude that is a function of the wind speed[26]. The exact cut-off height is very important[27] in the prediction of the occurrence of mirages (a condition when (part of) an object is seen more than once by a single sensor and/or with different than the original intensity). Therefore, efforts are presently underway to extend and improve the near-surface module of EOSTAR.

The current version of EOSTAR uses a single set of locally defined meteorological data, which is equivalent to assuming horizontal homogeneity. However, EOSTAR can easily be extended to work with multiple meteorological data sets along the range of interest.

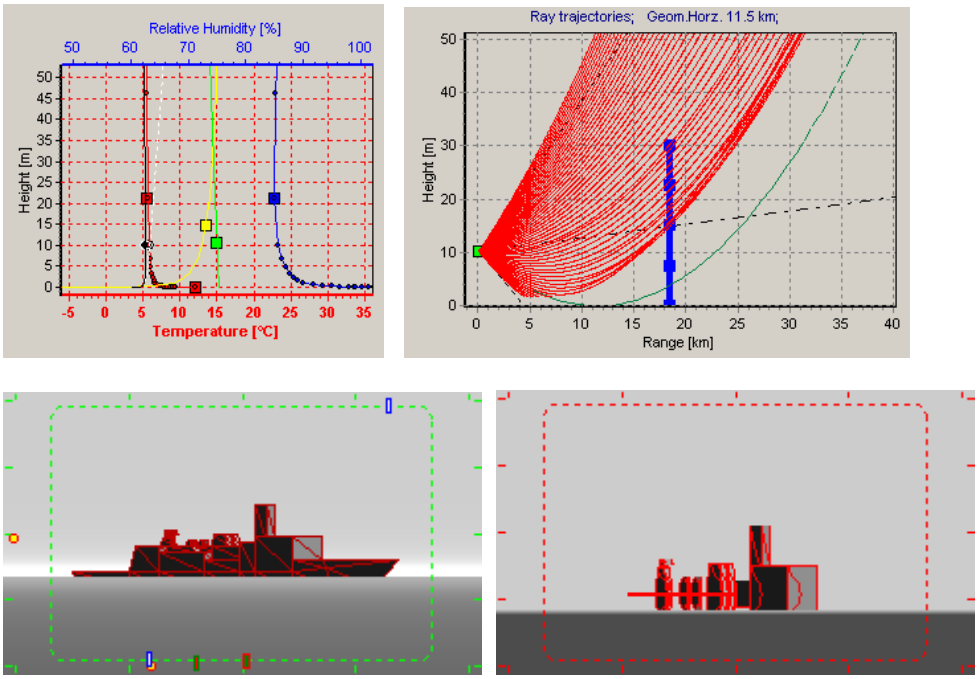


*Figure 1. The upper left panel is part of the graphical input module for bulk models. The square symbols refer to the user-specified meteorological input data. Also shown are the vertical profiles calculated by the bulk model. The upper right panel shows the ray trajectories in this atmosphere for a camera at a height of 10 m. The solid line is a representation of the height and location of a distant target (see lower panels). The left lower panel shows the target in a non-refracting atmosphere (reference view) and the lower right panel the same target in the refracting atmosphere defined by the upper right panel. The contour lines in the lower panels indicate the individual structural elements of the target. The images in the lower panels only show refractive effects, no turbulence, transmission or radiative effects.*

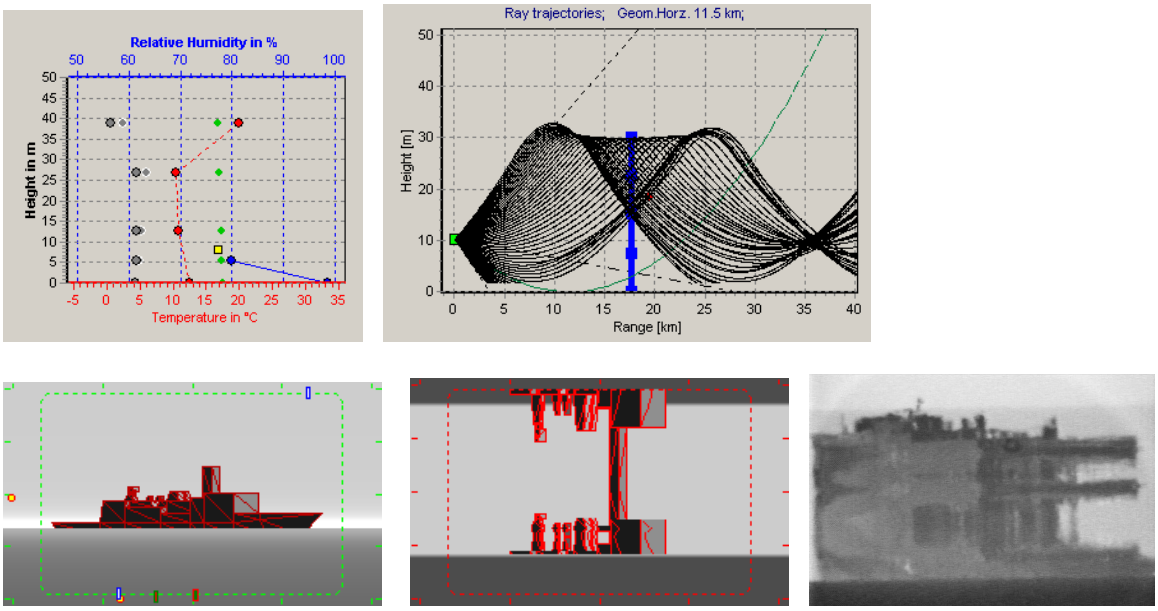


*Figure 2. As figure 1, except that the user has manually defined the profiles of temperature and humidity without invoking the bulk models. The lower-right panel shows an actual image recorded with a visual camera (SPAWAR Systems Center San Diego, Santa Ana conditions, target range approximately 20 km) for comparison. The meteorological conditions for the actual image are not exactly known.*

EOSTAR also allows calculating and visualizing the ray trajectories starting from a secondary camera located on the target and aiming backwards into the direction towards the primary camera. These trajectories will differ when the two sensors are not at the same height. Consequently, the forward and backward ray trajectories result in different atmospheric transfer functions (see below) although, following Fermat's principle[28], at least one fraction of both ray trajectories follows the same paths.

### 3.3 Horizon

The horizon is an indication of the maximum observation range of small objects near the surface. However, the horizon is not uniquely defined because atmospheric refraction causes the maximum observation range to be smaller or larger than can be expected on the basis of geometry only. Therefore, a distinction is made between the geometrical and the optical horizon.

The geometrical horizon is defined as the length of the straight line between the position of the camera and the farthest point where this line is tangent to the Earth, thus under the assumption of a non-refracting atmosphere (and for a flat sea surface). The geometrical horizon is invariant under the meteorological condition. This horizon is indicated in the upper right panel of Figure 1 by the green line. As an example, a target at 10 m height is 'above' the horizon at a range of 23 km.

The optical horizon, on the other hand, is defined as the distance between the camera position and the point where the ray with the lowest elevation angle is tangent to Earth (accounting for the wave height). Due to atmospheric refraction, this distance can be smaller or larger than the geometrical horizon. Under the meteorological conditions used to generate Figure 1, the optical horizon is given by the maximum range of the red lines (16 km for a target at 10 m height).

Often, terms denoted as sub- and super-refraction[29,30] are used to indicate whether the maximum observation range is respectively smaller or larger than under the standard atmospheric condition[30]. It should be noted, however, that the 'standard condition' does not correspond to a non-refracting atmosphere. Thus, the ray trajectories in a 'standard

atmosphere' are not simply straight lines but bent slightly towards the Earth due to the negative atmospheric pressure gradient. Compared to a non-refractive condition, a standard atmosphere is slightly sub-refractive, i.e., rays bend inward towards the Earth..

### 3.4 Atmospheric transfer functions

In a non-refracting atmosphere, the ray trajectories for the individual camera pixels are straight lines and their direction is independent of range. Images of targets are simply predicted by straightforward geometry (see the lower left panels of Figures 1 and 2). In a refracting atmosphere, on the other hand, the ray trajectories are bent according to Snell's law. The construction of images of distant targets then requires the height distribution of the rays at the location of the target. The atmospheric transfer functions compare ray heights or ray directions in refracting and non-refracting environments (for a selected target range). For instance, the relationship between the heights of the rays in a refracting and in a non-refracting atmosphere is an example of an atmospheric transfer function. Other possible transfer functions can be defined using combinations of vertical camera pixel row or ray index number, height of the rays above the surface, slope of the rays and variation of the height and slope with the ray-index number. All these 'transfer functions' are directly derived using the ray trajectory data and they are updated immediately when the position of the target is changed. Within EOSTAR, the user can currently select between 9 different types of transfer functions.

Figure 3 shows two atmospheric transfer functions for ranges of the targets as shown in Figures 1 and 2 (18.5 km and 17.5 km respectively). The transfer function in the left panel indicates that the minimum observation height from the position of the sensor is about 15 m above the sea level. Furthermore, the knee in the curve indicates that part of the target, between 15 m and 20 m height, is imaged twice: first inverted and next erect. The negative values for the 'non refracted heights' along the horizontal axis indicate that one would expect images from parts of the sea surface with the lowest 30 % of the camera pixels. The remainder of the transfer function is more or less a straight line with a slope of approximately 1, which indicates that there is no more distortion for objects above 20 m height. The transfer function in the right panel indicates that more distortion is present for the meteorological conditions of Figure 2. Half of the chart has a positive slope, indicating an erect image and the other part has a negative slope, indicating an image that is inverted. In more detail, this chart shows that parts of the target, between about 15.8 m and 17.8 m height, are imaged 4 times. As can be seen in the lower center panel of Figure 2, this corresponds to the stack of the ship.

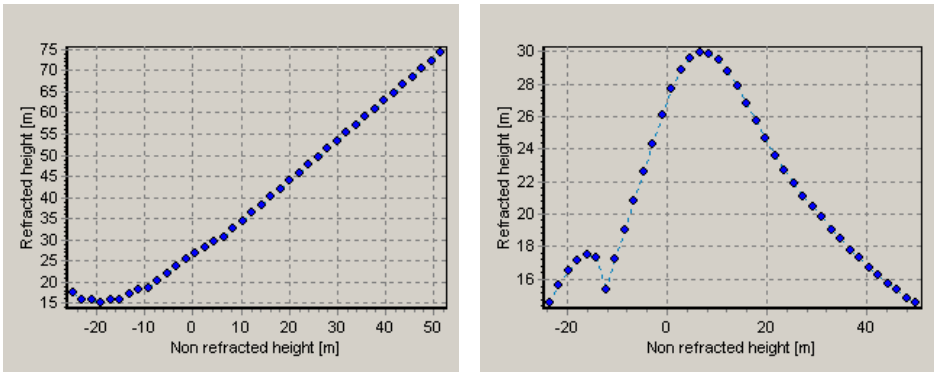


*Figure 3: Atmospheric transfer functions for the ray heights at the position of the targets shown in Figures 1 and 2.*

### 3.5 Transmission

Atmospheric transmission losses, which reduce the amount of target radiation reaching the camera aperture and consequently limit the detection range, are caused by scattering and absorption of radiation both by atmospheric molecules and aerosols. Molecules mainly absorb radiation, and the absorption varies strongly with wavelength, especially in the IR. Air temperature and humidity are the primary meteorological conditions that determine the molecular absorption. Aerosols, on the other hand, predominantly scatter radiation and their presence in the marine

surface layer is strongly related to the wind speed. Thus, the meteorological conditions play an important role for assessment of the atmospheric transmission losses.

Within EOSTAR, the molecular transmission losses are calculated using the external program MODTRAN[5] (**MOD**erate resolution **TRAN**smittance Code). MODTRAN is not part of EOSTAR and must be ordered separately. This program provides the spectral atmospheric transmission, path- and background radiance with a maximum resolution of 2 $cm^{-1}$, which is sufficient for our application. It should be noted, however, that a large number of input parameters must carefully be selected to obtain the proper output. This is not a straightforward process[31]. To aid the user, EOSTAR automatically prepares the MODTRAN input file, calls MODTRAN and takes care of the necessary analysis of the MODTRAN output data file (background- and path-radiation are also calculated by MODTRAN, see next section).

Aerosol transmission is calculated using ANAM, the **A**dvanced **N**avy **A**erosol **M**odel[32], which replaces and extends the well-known predecessor NAM[33] (**N**avy **A**erosol **M**odel). ANAM predicts the aerosol size distribution for heights up to 30 m in the marine surface layer as a function of wind speed, relative humidity, and air mass parameter, and calculates the vertical profile of the spectral extinction coefficient for the marine aerosol.

Compared to other processes in EOSTAR, the external programs MODTRAN and ANAM are much slower in generating the required output (on the order of seconds in-stead of fractions of seconds). Therefore, updating of the transmission is not done automatically after changing one of the input parameters, but needs to be activated explicitly by the user after specification of the input parameters. To further save time, EOSTAR calls MODTRAN and ANAM at a fixed number of heights and subsequently interpolates these spectral transmission data for other heights to calculate path-integrated transmission losses along each ray. The required processor time to calculate the path-integrated spectral transmission using this interpolation process is negligible compared to calls to MODTRAN and ANAM.

### 3.6 Background- and path radiation

EOSTAR uses MODTRAN (must be ordered separately) to evaluate the spectrally resolved path and background radiance for each ray. These spectra are required to generate radiometrically correct images, as well as, to calculate the contrast of possible targets on the sensor. The spectral background radiance is calculated as a function of elevation angle over the vertical field-of-view of the camera. This approach is necessary because the type of background (sky and sea, and, therefore, the spectra) and the intensity of the background changes considerably with elevation angle.

Path radiance is caused by atmospheric particles and molecules, which scatter radiation that does not originate from the target in the direction of the camera. This reduces the contrast of the target against its background. Ultimately, for targets at long ranges, the path radiance becomes equal to the background radiance. The spectral path radiance must be calculated over the path between target and camera, and over the (-vertical-) extent of the target.

There are several limitations and inconsistencies between the approaches outlined above. As an example, the calculation of the background does not yet include spatial variations (e.g., broken clouds). Furthermore, MODTRAN utilizes NAM to assess the aerosol concentration, whereas our transmission calculations utilize ANAM. Consequently, transmission and radiance calculations are made for different concentrations of aerosol. Likewise, the ray tracer in MODTRAN is slightly different from the ray tracer in EOSTAR, and sometimes the one code finds that a particular ray ends in the water, whereas the other code finds that the ray ends in the sky. Tools are currently being developed to remedy these shortcomings.

## 4. RESULTS VISUALIZATION

EOSTAR provides a large number of different output data (some examples are shown in Figures 1 through 3). The presentation of these data constitutes the ‘back end’ of the program, and is customized to the needs of a specific user. Most of the data can be directly copied to the Windows clipboard and pasted in other applications, or sent to a printer for making hard copies, or stored to disk.

EOSTAR provides output at different levels. First, the internal bulk models provide direct insight in the micrometeorological condition of the current atmospheric condition, based on the standard meteorological input data. Results of six different models are instantaneously available after each change of the input data and can be used to compare different bulk models at a single glance. The results of one of the models are used for further calculations, in particular to calculate the vertical profiles of the refractive index and the refractive index structure parameter $C_n^2$.

The ray trajectories or the observation paths of the camera pixels, which are derived from the vertical profile of the atmospheric refractive index, as well as the atmospheric transfer functions, can be considered as a second output data set.

Based on these ray trajectories and the vertical profiles of temperature, humidity and refractive index structure parameter, EOSTAR calculates the path-integrated and spectrally-resolved transmission, background- and path-radiation, as well as, the scintillation and blur for a point source at a selected position of a distant point target. All these data, which can be considered as third level data, have been summarized in a small monitor form on the screen for easy access. Furthermore, EOSTAR has a number of pre-programmed extended targets that can be placed anywhere in the user-defined space and viewed from any aspect angle to study the atmosphere effects on IR imaging. These targets are constructed from triangles, which can be given several properties such as temperature and spectral emission coefficient. With this information and the spectrally resolved atmospheric transmission, background and path radiation it is possible to simulate a true spectral image of a target in the scene as seen by the sensor system and to calculate the radiance or contrast for the selected aspect angle.

A unique and very powerful element of the EOSTAR modeling suite is the inclusion of several stand-alone modules, or tools. These tools provide more detailed information on various aspects of atmospheric propagation. There is a relatively simple interface to MODTRAN that calculates and displays the spectrally resolved molecular transmission, background radiation and path radiation based on a user-defined input data set. This interface can be coupled to the selected bulk model for the necessary meteorological input data. A second tool based upon ANAM enables a visualization of the change in the model particle size as a function of the input parameters. This permits the user to vary any of the four primary input parameters to see immediately the effect on the size distribution and the spectral extinction properties. The graphics user interface to ANAM is shown in Figure 4. The right graph gives the possibility to change wind speed, humidity, height and air mass parameter simply by dragging the symbols whereas the left graph gives the spectral distribution of the aerosol. A provision is made to switch instantaneously between number, area and volume distribution.

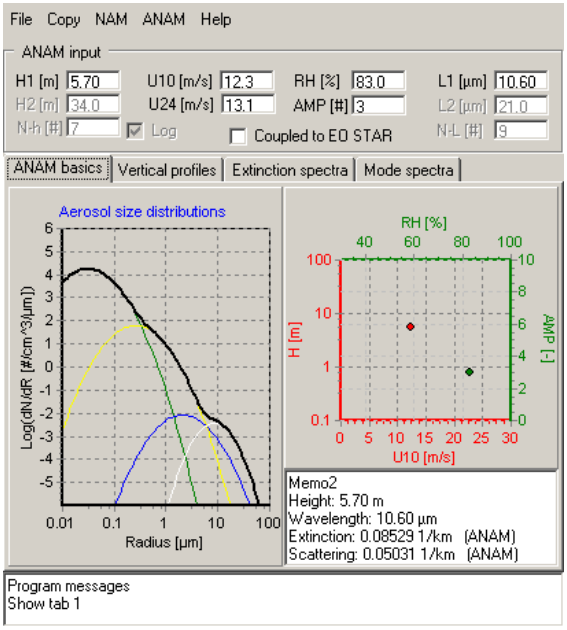


*Figure 4: Graphics user interface for the marine aerosol module ANAM. This tool provides the aerosol spectra (number, area or volume) and the vertical profile of the spectrally resolved extinction coefficient.*

The bulk models input module (shown in Figure 1) also constitutes a separate tool, which provides instantaneously vertical profiles of air temperature, humidity, wind speed and pressure on the basis standard (bulk) meteorological observations. In addition, this module gives also instantaneously the numerical results of six commonly used micrometeorological models based on these observations, which is very helpful to compare the performance of the different models and to make a proper decision for using a specific model.

Other tools provide information that may be helpful to set parameters for certain types of calculations, such as the detection range of a particular target. A tool developed around the equations of Planck's law calculates the emittance, radiance, and peak wavelength of a black body radiator on the basis of temperature and vice versa. Furthermore, if the size of the target is defined, the total or band-integrated radiation and intensity are calculated under the assumption that the source can be considered as a point source. The design of the tool is such that all processes work forward- and backward and that the user is informed of any lack in the information flow. Furthermore a tool is provided to calculate properties of wind driven sea waves and a tool to calculate the surface temperature and IR emission of high-speed air borne targets.

## 5. VALIDATION

Results generated by EOSTAR have been compared with theoretical and experimental data available from literature. First, the default bulk micrometeorological model was tested[12] and it was shown that the results are in excellent agreement with earlier published data[2]. Subsequently, the performance of the ray tracer and the module that generates synthetic images of point sources was compared with experimental data available from literature[34,35,36,37,38,39,40] to verify horizon, mirage images, and maximum intervision ranges. This comparison shows that there is a very good agreement between the experimental results and the same data generated by EOSTAR on the basis of bulk meteo data. Comparison with other experimental data[41,42,43,44] both for geometric effects and turbulence effects is currently underway and is promising. The validation efforts will be reported in full detail in a different manuscript.

## 6. CONCLUSIONS

An initial version of the computer program EOSTAR has been developed to simulate visual and IR images of targets in the marine surface layer. The basis for this program is formed by (bulk) meteorological parameters like air temperature, humidity, pressure, wind speed, and water temperature, and the properties of a selected camera system. Vertical profiles of the refractive index $n$ and the refractive index structure function $C_n^2$, required to predict atmospheric refraction and turbulence respectively, are calculated using the Monin-Obukhov similarity theory. Using these profiles, EOSTAR calculates ray trajectories, atmospheric transfer functions, geometrical and optical horizon, scintillation, blur and, finally, a simulated image of a selected target. Although the program is rather large, the update of this simulated image is almost instantaneously after changing one of the input parameters.

Spectrally resolved transmission, background and path radiance are calculated using calls to the external programs MODTRAN and ANAM. However, in comparison with other EOSTAR processes, these external programs are relatively time-consuming, requiring a few seconds to generate the desired output. Therefore, these parameters are only updated at the user's request and the external codes generate small data sets, which in turn are interpolated to obtain the path-integrated transmission, path and background radiation. These additional parameters, together with the intrinsic radiance of the target, allow simulating radiometrically correct images of targets as seen by the sensor.

EOSTAR has a user-friendly interface, is completely mouse-driven, runs under Windows on a standard PC and requires no special installation routines. (However, in order to access the MODTRAN molecular routines, the user must have installed the MODTRAN code, available from ONTAR[45].) The following versions of MODTRAN have successfully been used with EOSTAR: Mod3, Mod315, Mod3p5, Mod371, Modtran4, Mod4r01, Mod4vr0 and PcModwin. Users can access and modify most of the program parameters (e.g., define their own camera systems), and provisions have been made to handle large input data files for automatic analysis. Future developments will focus on an improved description

of the propagation environment (e.g., the near-surface region), as well as on the customization of the user-interface to meet specific requirements of (potential) customers.

## REFERENCES


1. R.B. Beland, "Propagation through atmospheric turbulence", in *The Infrared & Electro-Optical Systems Handbook,* Volume 2, *Atmospheric Propagation of Radiation*, pp. 157-234, edited by F.G. Smith, Ann Arbor, Michigan, USA: Infrared Information Analysis Center. 1993.
2. S.D. Smith, "Coefficients for sea surface wind stress, heat flux, and wind profiles as a function of wind speed and temperature", *J. Geophys. Res*, **93**, no C12, 15.467-15.472, 1988.
3. K.L. Davidson, G.E. Schacher, C.W. Fairall and A.K. Goroch, "Verification of the bulk method for calculating over water optical turbulence", *Appl. Opt*., **20**, 17, pp. 498-502, 1981.
4. W.T. Liu, K. Katsaros and J. A. Businger, "Bulk parameterization of air-sea exchanges of heat and water vapor including the molecular constraints at the surface*", J. Atmos. Sci*., **36**, pp. 1722-1735, 1979.
5. Web site to MODTRAN: Air Force Research Laboratory (AFRL), web site: www.vs.afrl.af.mil/Division/VSSSE/.
6. G.J. Kunz, "ARTEAM, Advanced ray tracing with Earth atmospheric models", in SPIE Proceedings 4718, *AeroSense 2002, Conference on Targets and Backgrounds VII: Characterization and Representation*, edited by W.R. Watkins, D. Clement and W.R. Reynolds, pp 397-404, SPIE, Bellingham, Washington, USA, 1992.
7. H. Tennekes and J.L. Lumley, "*A first course in turbulence*", The MIT Press, Cambridge, pp. 300, 1972.
8. S.P. Arya, "*Introduction to micrometeorology*", Academic Press, Inc., San Diego, pp. 307, 1988.
9. R.B. Stull, "*An introduction to boundary layer meteorology*", Kluwer Academic Publishers, Dordrecht, pp. 666, 1988.
10. C.A. Paulson, "The mathematical representation of wind speed and temperature profiles in the unstable atmospheric surface layer", *J. of Appl. Meteorol.*, **9**, pp. 857-861, 1970.
11. J. Kondo, "Air-sea bulk transfer coefficients in diabetic conditions", *Boundary-Layer Meteorol*, **9**, pp. 91-112, 1975.
12. G.J. Kunz, "A bulk model to predict optical turbulence in the marine surface layer", TNO Physics and Electronics Laboratory, The Hague, The Netherlands, Report TNO-FEL-96-A053, pp. 73, 1996.
13. C.W. Fairall and S.E. Larsen, "Inertial-dissipation methods and turbulent fluxes at the air-ocean interface", *Boundary-Layer Meteorol.*, **34**, 287-301, 1986.
14. J.C. Wyngaard, Y. Izumi and S.A. Collins, "Behavior of the refractive-index-structure parameter near the ground", *J. Opt. Soc. Am*., **61**, 1646-1650, 1971.
15. R.J. Hill, G.R. Ochs, and J.J. Wilson, "Measuring surface-layer fluxes of heat and momentum using optical scintillation", *Boundary-Layer Meteorol*., **58**, 391-408, 1992.
16. B. Edlén, "The dispersion of standard air", *J. Opt. Soc. Am.*, **43**, 5, pp.339-43, 1953.
17. B. Edlén, "The refractive index of air", *Meteorol.*, **2**, pp. 71-80, 1966.
18. Y.A. Kravtsov and Y.I. Orlov, "*Geometrical optics of inhomogeneous media*", Springer, Berlin, Heidelberg, New York, 1990.
19. W.G. Rees, C.M. Roach and C.H.F. Glover, "Inversion of atmospheric refraction data", *J. of the Opt. Soc. of Am*., **8**, 2, pp. 330-338, 1991.
20. S.Y. van der Werf, "Ray tracing and refraction in the modified US1976 atmosphere", *Appl. Opt*., **42,** 3, pp. 354-366, 2003.

21. J.M. Pernter and F.M. Exner, "*Meteorologische Optik*", Wilhelm Braumüller, Univesitäts-Verlagsbuchhandlung, Wien/Leipzig, pp. 907, 1922.

22. W.H. Lehn, "A simple parabolic model for the optics of the atmospheric surface layer", *Appl. Math. Mode*l., **9**, 12, pp. 447-453, 1985.

23. A.B. Fraser and W.H. Mach, "Mirages" in *Light from the sky*, edited by J Walker, Scientific American articles, pp.29-37, 1980.

24. M. Minneart, "*Light & color in nature*" (sections 39-46), Thieme & Cie Zutphen, 1974.

25. D.K. Lynch and W. Livingston, "*Color and light in nature*", Cambridge, University Press, Cambridge, pp. 254, 1995.

26. M.A. Donelan and W.H. Hui, "Mechanics of ocean surface waves", in *Surface waves and fluxes*, edited by G.L. Geernaert and W.J. Plant, pp 209-246, Kluwer Acad., Norwell, Mass., 1990.

27. L.J. Navarro, A.M.J. van Eijk, G.J. Kunz, A. Phelippeau-Gosselin and P.G. Mestayer, "Influence de la couche atmosphérique marine sur la propagation électrmagnétique", 4ièmes Journées d'études *Propagation électromagnétique du décametrique à l'angström*, 13-15 March, Rennes, France, 2002.

28. F.A. Jenkins and H.E. White, "*Fundamentals of optics*", McGraw-Hill, New York, pp. 637, 1957.

29. H.V. Hitney, " Refractive effects from VHF to EHF; Part A: Propagation mechanisms", in *Propagation modeling and decision aids for communications, radar and navigation systems*, edited by K.H. Craig, pp. 4A.1-4A.13, AGARD 92200 Neuilly-Sur-Seine, France: AGARG-LS-196, 1994.

30. J.R. Rottier, J.R. Rowland, G.C. Konstanzer, J. Goldhirsh and G.D. Dockery, "APL environmental assessment for Navy anti-air warfare", *John Hopkins APL Technical Digest*, **22**, 4, pp. 447-461, 2001.

31. A. Berk, et al., "*MODTRAN4 user's manual*". Hanscom AFB, MA, 01731 – 3010, Air Force Research Laboratory - Space Vehicles Directorate - Air Force Materail Command, 1999.

32. A.M.J. van Eijk, L.H. Cohen, L.J. Navarro and G. de Leeuw, "Near-surface aerosol transmission in the marine environment", in SPIE Proceedings 4848, *Optics in atmospheric propagation and adaptive systems V*, edited by A. Kohnle and J.D. Gonglewski, pp. 160-169, SPIE, Bellingham, Washington, USA, 2002.

33. S.G. Gathman, "Optical properties of the marine aerosol as predicted by the Navy aerosol model", *Opt. Eng.*, **22**, pp. 57-62, 1983.

34. J.L. Forand, D. Dion, and J. Bealieu, "MAPTIP: Canada's measurements of refraction effects", in *AGARD: Symposium on Propagation Assessment in Coastal Environments*, edited by D.H. Höhn, pp. 24.1-24.6, AGARD-CP-567, Bremerhafen, Germany, 19-22 September 1994.

35. J.L. Forand, "MAPTIP: refractive effects in the visible and IR", in in SPIE Proceedings 2828, *Image propagation through the atmosphere*, edited by J.C. Dainty and L.R. Bissonnette, pp. 39-49, SPIE, Bellingham, Washington, USA: SPIE, 1996.

36. J. Claverie, Y. Hurtaud, D. Dion, L. Forand and P. Mestayer, "Influence of meteorological models on tefractivity profiles computation in the marine boundary layer", in *Propagation electromagnetique dans l'atmosphere du decametrique a l'Angstrom* edited by L.B.A. Junchat, Rennes, France, 7-9 October 1997.

37. J. Claverie, B. Tranchant, P. Mestayer, A.M.J. van Eijk and Y. Hurtaud, "Effets de la refraction atmospherique sur la propagation infrarouge dans la basse atmosphere marine comparaison des modeles SeaCluse er PRIAM" in *E-O propagation, signature and system performance under adverse meteorological conditions considering out-of-area operations*, NATO, RTO-MP-1/AC/323/(SET)TP/2, Naples, Italy, 16-19 March 1998.

38. K. Stein, "Characteristics of ship borne targets in warm coastal environment in mid and long wave IR", in SPIE Proceedings 3494, *Optics in Atmospheric Propagation and Adaptive systems II*, edited by A. Kohnle and A.D. Devir SPIE, Bellingham, Washington, USA, 1998.

39. K. Stein, “Analysis of an airborne target over sea”, in SPIE Proceedings 3494, *Optics in Atmospheric Propagation and Adaptive systems II*, edited by A. Kohnle and A.D. Devir SPIE, Bellingham, Washington, USA, 1998.

40. K. Stein, “LAPTEX 1996: Analysis of an airborne target over sea”, in SPIE Proceedings 3494, *Europto Conference on Optics in Atmospheric Propagation and adaptive Systems IV,* edited by A.D. Devir, A. Kohnle, U. Schreiber and C. Werner, pp. 60-72, SPIE, Bellingham, Washington, USA, 1996.

41. D.R. Jensen, S.G. Gathman, C.R. Zeisse, C.P. McGrath, G. de Leeuw, M.H. Smith, P.A. Fredrickson, K.L. Davidson, “Electro-optical propagation assessment in coastal environments (EOPACE): summary and accomplishments”, *Opt.* E*ng*., **40**, pp.1486-1498, 2001.

42. K. Stein, E. Polnau and D. Seiffer, “IR Propagation through the marine boundary layer - Comparison of model and experimental data”, in SPIE Proceedings 4884, *Optics in Atmospheric Propagation and Adaptive Systems V*, edited by A. Kohnle and Gonglewsk Gonglewsk*,* SPIE*,* Bellingham, Washington, USA, 2002.

43. A.N. de Jong, H. Winkel, M.M Moerman, K. Stein, K. Weiss-Wrana, L. Forand, G. Potvin, J. Buss, A. Cini, H. Vogel, E. Startk, “TG16 point target detection experiment POLLEX, Livorno 2001” in SPIE Proceedings 4820, *Infrared Technology and Applications XXVIII*, edited by B.F. Andresen, G.F. Fulop and M. Strojnik*,* SPIE*,* Bellingham, Washington, USA, 2002.

44. A.N. de Jong and H. Winkel, “Enhanced IR point target detection by atmospheric effects” in SPIE Proceedings 4820, *Infrared Technology and Applications XXVIII*, edited by B.F. Andresen, G.F. Fulop and M. Strojnik*,* SPIE*,* Bellingham, Washington, USA, 2002.

45. Web side ONTAR, www.ontar.com/prod_PCModWin.htm.